ACS APPLIED POLYMER MATERIALS

pubs.acs.org/acsapm Article

Structure–Mechanical Property Relationships of 3D-Printed Porous Polydimethylsiloxane

Rebekah Woo,‡ Grace Chen,‡ Jiayu Zhao,‡ and Jinhye Bae*

Cite This: *ACS Appl. Polym. Mater.* 2021, 3, 3496–3503 Read Online

ACCESS | Metrics & More | Article Recommendations | Supporting Information

ABSTRACT: Polydimethylsiloxane (PDMS) is one of the most commonly used silicone polymers due to its low cost, optical transparency, flexibility, chemical inertness, and biocompatibility. As a subset of PDMS, porous PDMS shows great potential across a large variety of applications in fields such as biomedical engineering, shock absorption, and oil/water separation. However, the conventional method to fabricate porous PDMS (i.e., molding) has limited geometric complexity. Thus, precursor formulations (i.e., inks) of porous PDMS have been studied to enable three-dimensional (3D) printing to increase the design space of more complex structures. Despite the recent advances in such areas, the relationship between mechanical properties and structural parameters of porous PDMS has yet to be reported. Herein, we study the mechanical properties of porous PDMS as a function of the print patterns and infill densities to demonstrate the highly tunable mechanical properties of printed porous PDMS via direct ink writing. To enable 3D printing of PDMS, we develop a porous PDMS ink consisting of a PDMS precursor, silicone oil, dibutyl phthalate (DBP), and fumed silica nanoparticles by tuning the rheological behaviors. The porous structures in PDMS are subsequently generated by the removal of DBP in the cured PDMS matrix and characterized by scanning electron microscopy. Mechanical characterization exhibits that the printed sample using the porous PDMS precursor has enhanced stiffness, strength, toughness, and ductility compared to the nonporous PDMS sample. Notably, a broad range of mechanical properties is achieved by varying structural parameters (i.e., infill densities and printing patterns) for 3D printing of a single porous PDMS material system, which provides insight for designing adaptive soft robots and actuators that can integrate different mechanical properties into a single device by simply changing the structural parameters.

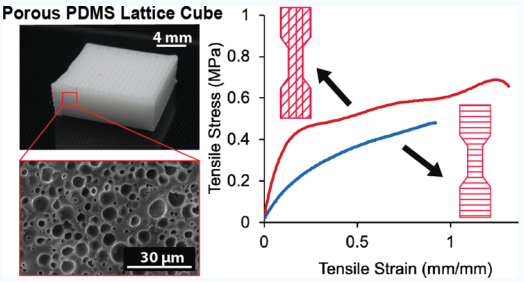

KEYWORDS: *polydimethylsiloxane, porous materials, 3D printing, direct ink writing, mechanical properties, rheology*

INTRODUCTION

Polydimethylsiloxane (PDMS) has been widely used as an inexpensive silicone polymer due to various advantages including optical transparency, flexibility, chemical inertness, and biocompatibility.[1−3] It has been considered an important material to study in industrial and fundamental research for applications ranging from mechanical[4] and electrochemical sensors,[5] microfluidics,[6] and soft lithography[7] to antifoaming agents[8] in foods and cosmetics. Moreover, porous PDMS is emerging as a useful material in recent years for applications in multiple fields, such as scaffolding for soft tissue engineering,[9] wearable electronics,[10] shock absorption,[11] and oil/water separation,[12] since its highly porous structure provides a large surface area to volume ratio and improves elasticity and flexibility. In this regard, the design and fabrication of complex three-dimensional (3D) structures are required to further push the boundary of advanced applications. However, porous PDMS has been conventionally fabricated via mold casting, which involves multiple steps and tools with limited structure complexity and feature sizes.[13,14]

3D printing is a distinguished, mold-free manufacturing method that has evolved remarkably in the past decade due to fast prototyping, ability to fabricate complex geometries, and freedom of design.[15,16] Among 3D printing, direct ink writing (DIW) is a promising technique to pattern versatile materials in three-dimensions via a layer-by-layer extrusion process, allowing for more intricate designs and finer feature size (down to ∼250 μm) than traditional mold-cast objects.[17] However, it has been challenging to print liquid polymer precursors using DIW due to the requirement of shear thinning behavior and yield stress,[18] which have become bottlenecks for developing 3D-printable precursor formulations. In previous studies, a PDMS precursor containing fumed silica nanoparticles (NPs) has been directly printed out to fabricate soft autonomous robots,[19] synthetic spider webs,[20] and 3D perfusion chips.[21] The hydrogen bonds formed within the silanol groups on the silica surface create a network in the PDMS precursor ink,

Received: April 5, 2021
Accepted: June 11, 2021
Published: June 25, 2021

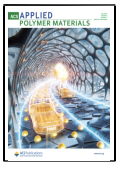

https://doi.org/10.1021/acsapm.1c00417
ACS Appl. Polym. Mater. 2021, 3, 3496–3503

which is responsible for the achievement of the desired rheological properties.[22] Fabrication of porous PDMS via DIW has also been reported by incorporating gas microballoon pore formers,[23] fugitive particles,[24] or phase.[25] However, despite recent advances in designing a porous PDMS ink formulation that allows 3D printing, the relationship between mechanical properties and structural parameters of porous PDMS has not been fully explored yet. Very recently, Mea et al. demonstrated the DIW of porous PDMS with droplet inclusions. The mechanical properties of PDMS were found to be dependent on the constituents and relative proportions of the droplet phase in which the included droplets lead to the softening of PDMS.[26] Exploiting such structural principles is crucial for designing appropriate structures with desired mechanical properties for particular applications. Furthermore, it also allows for the fabrication of adaptive soft actuators and robots with spatially tuned mechanical properties by structural printing parameters which potentially modulate their motion and 3D shape transformation.[27]

Here, we demonstrate the highly tunable mechanical properties of the printed porous PDMS by varying structural parameters (i.e., print patterns and infill density). For DIW porous PDMS, we develop a porous PDMS ink with shear thinning behavior and yield stress. It allows for the fabrication of porous PDMS into controlled 2D or 3D structures with both high fidelity and enhanced stiffness, toughness, strength, and ductility compared to the nonporous PDMS. Taking advantage of the great structural control offered by DIW,[17] we show that a broad range of mechanical properties can be readily achieved with different print patterns and infill densities using a single material system. We anticipate that the principles and strategies found in this work will provide new approaches for designing adaptive soft actuators and robots by allowing us to program and integrate different mechanical properties into a single device by simply changing the structural parameters. It may also benefit fields such as biomaterials[28] and medical applications[29] where complex 3D shapes created with porous PDMS are needed.

EXPERIMENTAL SECTION

Materials. The PDMS precursor and cross-linker (Sylgard 184) were purchased from Dow Corning. Dibutyl phthalate (DBP) was obtained from Spectrum Laboratory Products, Inc. Silicone oil (CAT #S159500) was purchased from Fisher Chemical. Fumed silica NPs (CAB-O-SIL EH-5, size: 0.2−0.3 microns) were purchased from Cabot Corporation. Ethanol (200 proof pure ethanol) and isopropanol were purchased from Koptec. (Tridecafluoro-1,1,2,2-tetrahydrooctyl)dimethylchlorosilane (silane) was purchased from Gelest Inc.

Preparation of Silane-Treated Glass Sides. Bare glass slides (75 mm × 50 mm × 1 mm) were first cleaned using isopropanol and placed into a vacuum desiccator after drying. Silane (2−3 drops) were added to the glass slide in the middle followed by vacuum evaporation for 7 h.

Preparation and 3D Printing of the Porous PDMS Precursor. The porous PDMS precursor was prepared by a simple one pot mixing process using a thinky planetary mixer (Thinky Inc., Thinky Mixer AR-100) under 2000 rpm mixing conditions. First, 3 g of PDMS base and 0.3 g of PDMS curing agent were mixed for 1 min. Subsequently, 0.675 g silicone oil was added and mixed for 1 min. DBP (3.675 g) was added and mixed for an additional 3 min. Lastly, 0.69 g silica NPs was added and mixed for 1 min.

The prepared precursor (6 mL) was first loaded into a 12 mL syringe and then mounted into the dispenser of the extrusion 3D printer (Rokit INVIVO). The precursor was printed onto the silane-treated glass slide using a 20 gauge needle. The silane-treated glass slide was used to prevent the cured samples from sticking to the glass slide and generating residual stress while peeling off, thus ensuring accurate results in tensile testing. The 3D printing process was conducted at a print speed of 10 mm/s. To prepare samples for the tensile test, a STL file of dog-bone shape with dimensions of 17 mm × 64 mm × 0.8 mm was created on 3D modeling software (Fusion 360) and uploaded to slicing software (New K Creator) built in the 3D printer. Infill density and print patterns were directly adjusted within the slicing software. For the dog-bone shape samples, two layers were printed out with a layer spacing of 0.4 mm for each. Different printing orientations were created by changing the angle at which the second layer was being printed with respect to the first layer. Total printing time varied upon the infill density and print pattern of the sample. After printing the porous PDMS precursor, the printed samples were thermally cured in an oven at 100 °C for 2 h followed by immersion in ethanol for 7 h to remove DBP. The samples were then transferred to an oven to fully evaporate the ethanol at 60 °C for 1 h.

Preparation and 3D Printing of the Nonporous PDMS Precursor. The nonporous PDMS precursor was prepared as a control sample. Similar to the porous PDMS preparation, 3 g of PDMS base and 0.3 g PDMS curing agent were mixed in a thinky planetary mixer for 1 min at 2000 rpm. Then, the nonporous PDMS precursor was placed into a desiccator for 15 min to remove air bubbles. The precursor ink (3 mL) was loaded to a 10 mL syringe and printed on the silane-treated glass slides using a 20 gauge needle, using the same printing parameters as the porous PDMS precursor. To prepare samples for the tensile test, the nonporous PDMS precursor was poured into dog-bone shaped molds with dimensions of 17 mm × 64 mm × 0.8 mm. After printing or casting of the nonporous PDMS precursor, the prepared samples were cured in an oven at 100 °C for 2 h.

Characterization. Stress−strain data were obtained using a universal testing machine (Instron Corp., Instron 3342) with a strain rate of 10 mm/s. Rheological data were obtained using an ARG2 rheometer (TA instruments). The viscosity measurements of both nonporous and porous PDMS precursors were set to a steady-state with a shear rate ranging from 0.1 to 100 s^{-1}. The modulus measurements were set to an oscillatory state with a shear rate ranging from 0.1 to 1000 s^{-1}. Optical micrographs were captured using an optical microscope (Keyence VHX1000). Images of the microporous structure were obtained using scanning electron microscopy (SEM) imaging (FEI Quanta FEG 250).

RESULTS AND DISCUSSION

Porous PDMS Precursor Preparation and Microstructure Characterization. Important rheological properties for designing DIW precursor ink are shear thinning behavior, yield stress, and storage modulus.[30] Shear thinning is crucial for DIW since it will facilitate the ink extrusion during the printing process. Sufficient yield stress (>50 Pa)[24,25,29] helps the ink to return to a solidlike material after deposition so that it is able to support itself and layers above.[31] Additionally, the storage modulus, a measure of the elastic response of a material, must be high enough so that the resulting structure is rigid, but not too high that the ink clogs the nozzle during extrusion.[32] To fulfill these criteria, we developed a porous PDMS ink composed of four components, including PDMS liquid resin (Sylgard 184, containing 10 wt % cross-linker), silicone oil (22.5 wt %), DBP (122.5 wt %), and fumed silica NPs (23 wt %). Silicone oil was added to dilute the PDMS precursor. DBP works as both a rheological modifier and a porogen. Upon mixing, the PDMS precursor and DBP form emulsions due to the immiscible nature in which DBP subsequently breaks into small droplets and spreads almost evenly throughout the PDMS precursor. This in turn creates micron-sized pores in the PDMS matrix after

https://doi.org/10.1021/acsapm.1c00417
ACS Appl. Polym. Mater. 2021, 3, 3496−3503

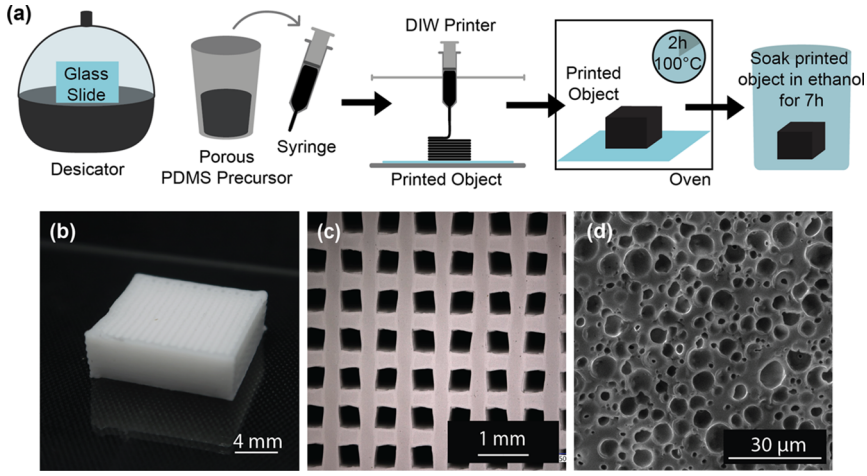

Figure 1. (a) Step-by-step process of the preparation and printing of the porous PDMS precursor. (b) Isometric view of the lattice cube structure printed using the porous PDMS precursor (dimensions: 13 × 13 × 4 mm). (c) Optical microscopy image of the lattice structure. (d) Cross-sectional SEM image of porous PDMS without silica NPs.

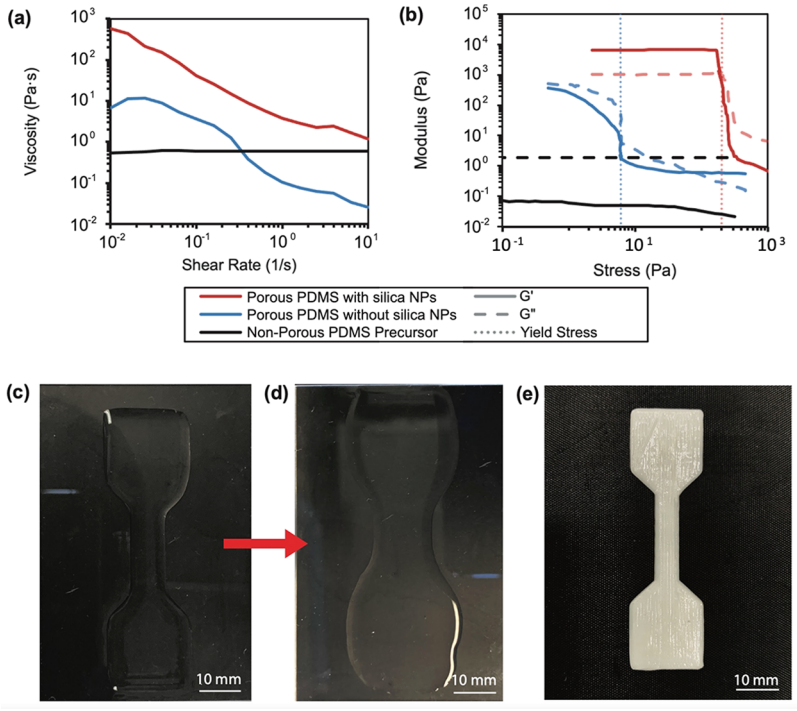

Figure 2. (a, b) Rheology test of the nonporous PDMS precursor (black solid line), porous PDMS precursor with 23 wt % silica NPs (red solid line), and porous PDMS precursor without silica NPs (blue solid line). The formula for the porous PDMS precursor without silica NPs is composed of the PDMS precursor, silicone oil, and DBP. (a) Plots of viscosity vs shear rate and (b) storage modulus (G') and loss modulus (G") vs stress. (c–e) Side-by-side comparison of printed samples by nonporous and porous PDMS precursors. The dog-bone shaped sample of nonporous PDMS (c) right after printing and (d) 1 h after printing that shows that the nonporous PDMS precursor is unable to retain the 3D-printed structure. (e) Dog-bone shaped sample of the porous PDMS precursor after printing that shows that it is able to maintain its shape even after 48 h at room temperature at which point the sample is fully cured.

removing DBP from the cured PDMS sample. Fumed silica NPs were added to further improve the rheological properties, as they endow the ink with shear thinning behavior, a yield stress point, and a higher storage modulus.

Figure 1a illustrates the fabrication process. The prepared precursor was first printed into the predesigned 3D structure on a silane-treated glass slide; then, the printed structure was thermally cured at 100 °C for 2 h. Upon curing, DBP and silicone oil were removed by soaking the sample in an ethanol bath, leaving micron-sized pores within the sample. To demonstrate the printing capability of the porous PDMS ink, we printed a lattice structure using a 20 gauge needle (see Supporting Information: Figure S1, Supporting Video 1). As shown in Figure 1b, the printed lattice structure is 13 × 13 × 4 mm in dimension and can hold its 3D structure remarkably well up to 48 h at which point the sample is already cured at room temperature. An optical microscopy image of the lattice structure shown in Figure 1c further supports the fact that the porous PDMS precursor can maintain high fidelity, as a well-defined lattice can be observed with a line-to-line (edge to

https://doi.org/10.1021/acsapm.1c00417
ACS Appl. Polym. Mater. 2021, 3, 3496–3503

edge) distance around 0.4 mm. Next, we performed SEM to investigate the microstructures of the porous PDMS sample. The cross-sectional view of the cured porous PDMS sample shows rough and irregular porous structures presumably due to the micron-sized agglomeration of the fumed silica NPs,[22] which does not clearly reveal the pores formed by the removal of DBP and silicone oil (see Supporting Information: Figure S2a). Thus, a porous PDMS sample without silica NPs (i.e., consisting of only the PDMS precursor, silicone oil, and DBP) was prepared to examine the porous structure and size generated by the removal of DBP and silicone oil from the cured sample. A cross-sectional SEM image of the sample without silica NPs before removing DBP and silicone oil using ethanol shows irregularly shaped cavities distributed throughout the sample (see Supporting Information: Figure S2b). After the removal of DBP and silicone oil through an ethanol bath, the micron-sized pores formed with spherical shape that minimize surface energy, as seen in the cross-sectional SEM image illustrated in Figure 1d. The micron-sized pores have diameters ranging from 0.8∼7.5 μm with an average value 2.4 ± 1.5 μm (see Supporting Information: Figure S3).

Rheological Properties of Nonporous and Porous PDMS. Rheological data support that the porous PDMS precursor possesses shear thinning and solidlike (G' > G") behavior with yield stress to retain its 3D structure with high fidelity after printing. As seen in Figure 2a, before any modification, the nonporous PDMS precursor exhibits low viscosity of 5.97 Pa·s with a typical Newtonian fluid behavior, as the viscosity does not change as shear rate increases. In addition, in Figure 2b, the value of loss modulus (G") is higher than that of the storage modulus (G'), meaning the nonporous PDMS ink possesses a liquidlike behavior. Upon adding DBP and silicone oil (i.e., without silica NPs), the ink starts to show shear thinning behavior, as the viscosity decreases as the shear rate increases (Figure 2a). Yield stress is observed at a value of 6.02 Pa in the modulus measurement (Figure 2b). However, G" is still larger than G' before yield happens, indicating a liquidlike behavior, which is not suitable for printing. Thus, fumed silica NPs were added to further improve the rheology properties to enable printing. The initial viscosity of the porous PDMS precursor increased from 67.12 to 5667 Pa·s after the addition of fumed silica NPs (Figure 2a). Furthermore, the precursor exhibits a greater yield stress value of 200.05 Pa with a solidlike behavior before the yield stress value (G' > G") (Figure 2b). With this high yield stress, the porous PDMS precursor can support its own weight and layer stacking three-dimensionally while printing.

To observe the behaviors of inks described in the rheological characterization above, dog-bone samples were 3D-printed using both the nonporous and porous PDMS precursor. As supported by the rheology analysis, Figure 2c−e shows that the nonporous PDMS precursor has poor fidelity and cannot maintain its printed structure. Figure 2c shows a low-fidelity dog-bone shape immediately after printing, and in Figure 2d, nonporous PDMS begins to spread out and lose its printed shape within 1 h after printing (see Supporting Information: Figure S4, Supporting Video 2), whereas, in Figure 2e, the printed porous PDMS precursor exhibits high shape definition and retains its printed shape until it is fully cured, which takes 48 h at room temperature.

Mechanical Properties of Nonporous and Porous PDMS. Porous PDMS compared to nonporous PDMS showcases a higher quality printing of 3D structures and improved mechanical properties. We conducted tensile testing to characterize the difference in Young's modulus (E), elongation at break, and ultimate tensile stress (UTS) between nonporous and porous PDMS. Young's modulus is a material's resistance to elastic deformation under load, which is determined from the initial slope of the strain−stress curve using Hooke's law, $E = \sigma/\varepsilon$, where σ is stress and ε is strain.[33] Elongation at break is determined from the strain at the fracture point of the strain−stress curve, representing how much a material will plastically and elastically deform before fracture. UTS is determined by the highest stress point of the strain−stress curve, which is the maximum stress a material can resist before tearing.

Figure 3 shows a representative tensile test curve of the printed porous PDMS sample with a 0−0 print pattern (e.g.,

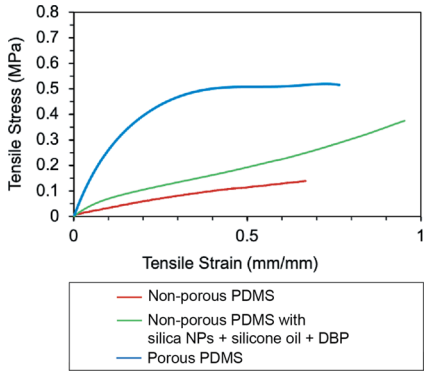

Figure 3. Stress−strain curves of nonporous PDMS (red), nonporous PDMS with silica NPs, silicone oil and DBP (green), and porous PDMS (blue) with 0−0 print pattern at 100% infill density.

0−0 means the first layer orientation is 0° and the second layer is 0° as well) at 100% infill density (where infill % = (volume of printed material/volume of object volume) × 100), nonporous PDMS and nonporous PDMS with silica NPs, silicone oil and DBP, respectively. As depicted in Figure 3, the Young's modulus of nonporous PDMS is 0.51 MPa, while the Young's modulus of porous PDMS is 2.44 MPa. The elongation at break for nonporous PDMS is 71%, which is 16% lower than porous PDMS which has a percent elongation of 85%. Notably, although porous PDMS has a significantly higher Young's modulus than nonporous PDMS, the pores in the PDMS matrix endow the sample with a high level of flexibility and deformability, resulting in a higher elongation at break value.[34] The UTS of nonporous PDMS is 80% lower than porous PDMS. It is also noted that the stress of nonporous PDMS increases at a steady rate during stretching without plastic deformation, as indicated by the linear path it travels in the plot, whereas porous PDMS undergoes a higher plastic deformation before breaking with a yield strain at 0.08 mm/mm (Figure 3), marking the point when the material begins to behave plastically. The curve also shows that the porous PDMS sample is tougher since it has a higher area under the curve (0.327 MPa) when compared to the curve of nonporous PDMS (0.055 MPa). To examine whether the enhanced mechanical properties of porous PDMS compared to nonporous PDMS are attribute to the presence of micron-sized pores, we prepared samples with the same composition to porous PDMS but with no pores inside. Such samples were denoted as nonporous PDMS with silica NPs + silicone oil + DBP in Figure 3 (green line). Young's modulus of which (0.84

https://doi.org/10.1021/acsapm.1c00417
ACS Appl. Polym. Mater. 2021, 3, 3496−3503

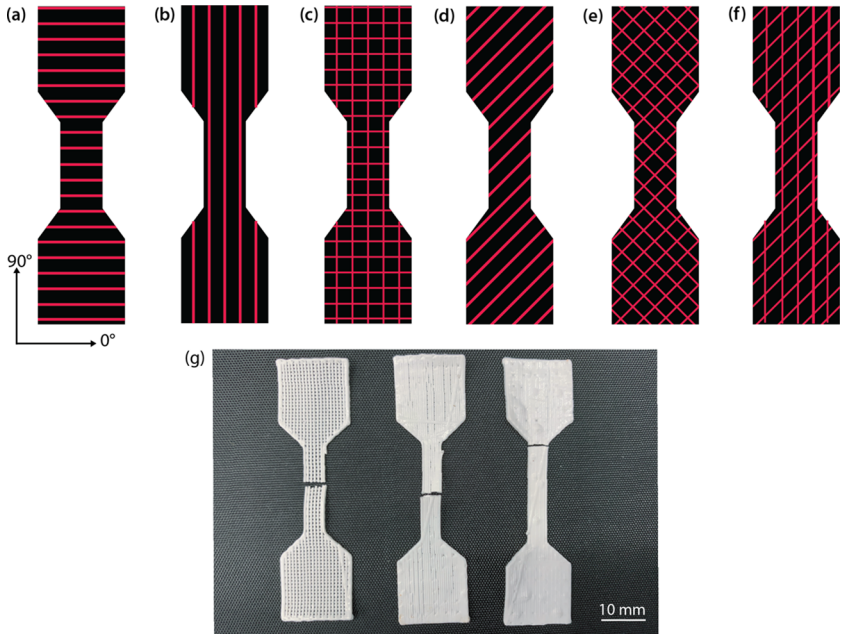

Figure 4. Printing dog-bone samples with different patterns for tensile testing. The dog-bone samples have dimensions of 17 mm × 64 mm × 0.8 mm. These print patterns are named according to the printing angle of the first and second layers, respectively: (a) 0−0, (b) 90−90, (c) 0−90, (d) 45−45, (e) 45−(−45), and (f) 90−45. (g) Printed porous PDMS dog-bone shape samples of 0−90 at 50, 75, and 100% infill density (from left to right) after tensile testing.

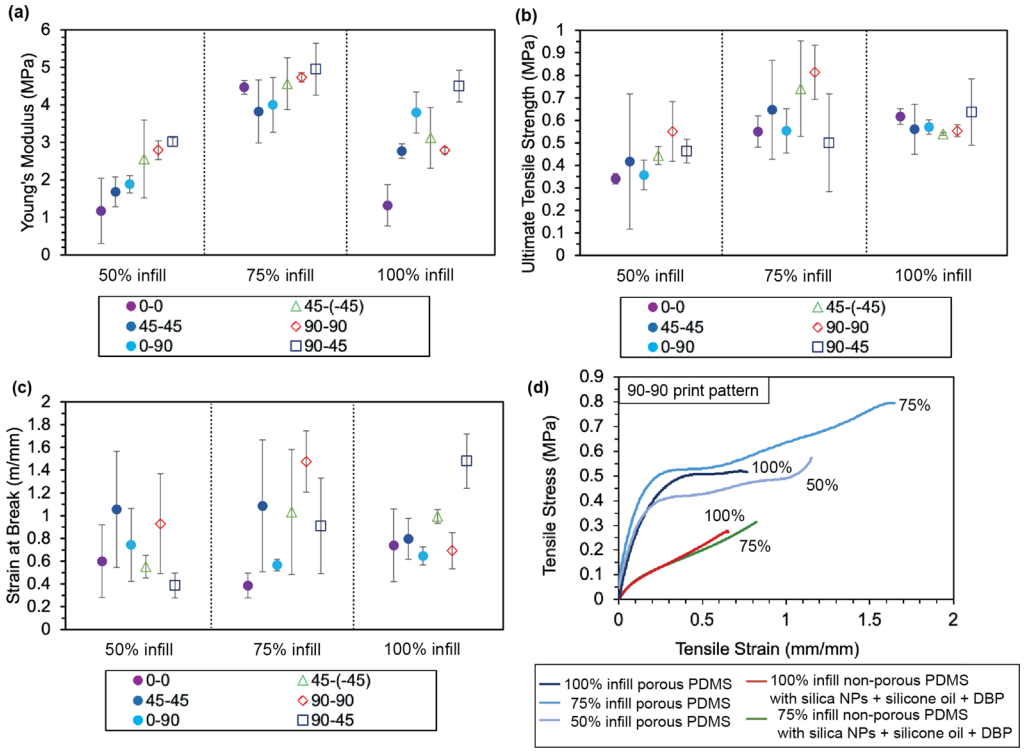

Figure 5. (a) Young's modulus values at 50, 75, and 100% infill densities with different print patterns reveal that samples with 75% infill density exhibit the highest Young's modulus on average. (b) Ultimate tensile strength values at 50, 75, and 100% infill densities with different print patterns also show the highest values at 75% infill density. (c) Strain at break values at 50, 75, and 100% infill densities with different print patterns show an increase from 50 to 75% infill density but no obvious trends between 75 and 100% infill density. (d) Stress−strain curves of porous PDMS and nonporous PDMS with silica NPs, silicone oil, and DBP printed in a 90−90 print pattern with different infill densities.

MPa) is slightly higher than nonporous PDMS (0.51 MPa) due to the addition of silica NPs, while it is more than 65% less than that of porous PDMS (2.44 MPa). The UTS of nonporous PDMS with silica NPs, silicone oil, and DBP is 26% lower than the porous PDMS. As for the elongation at break, nonporous PDMS with silica NPs, silicone oil, and DBP is 5% larger than porous PDMS. Given the fact that they have the same composition, the sample with internal pores is more

https://doi.org/10.1021/acsapm.1c00417
ACS Appl. Polym. Mater. 2021, 3, 3496−3503

prone to crack propagation than the one without pores.[35] Thus, porous PDMS exhibits a slightly smaller elongation at break value. Similar to nonporous PDMS, the strain−stress curve of nonporous PDMS with silica NPs, silicone oil, and DBP also exhibits a linear behavior, indicating that the plastic deformation observed in porous PDMS is solely determined by the micron-sized pores in the PDMS matrix. This characterization proves the enhanced stiffness, ductility, toughness, and strength of the porous PMDS samples.

Effect of the Print Pattern and Infill Density on Mechanical Properties of Porous PDMS. It is reported that print patterns have a noticeable influence on mechanical properties of fabricated samples. Most previous reports have been focused on different shapes of print patterns, such as rectilinear, honeycomb, and concentric patterns,[36−38] however the angle of the printed layers with respect to the direction of strain is often not taken into account. In addition to print patterns, infill density is also an important point to note when fabricating DIW objects since it determines the percentage of volume that is filled with material. To study the effect of the print pattern and infill density on mechanical properties of printed samples, dog-bone shape porous PDMS samples were printed with a certain infill density by varying print patterns and tensile tested as shown in Figure 4a−f. All patterns were printed with two layers and were named according to each layer's print orientation angle. An example of the dog-bone samples with various infill densities after the tensile test is shown in Figure 4g, with 0−90 printed at infill densities of 50, 75, and 100% from left to right.

During tensile testing, we observed that when the porous PDMS ink was printed parallel to the direction of loading, the sample was much stiffer than samples in which the ink was printed perpendicular to the direction of loading. Such results have been reported across previous studies as well.[39−41] Among six different print patterns (Figure 4a−f), the 90−45 sample shows the highest Young's modulus across all infill densities (Figure 5a). This high overall stiffness could be due to the 45° angle between printed layers. In all other samples, the second layer was either printed parallel or perpendicular to the first layer; however, the 90−45 has a 45° angle between layers, which creates a higher contact (i.e., bonding) area than print patterns that have 90° between the layers.[42] The layer oriented at 45° also allows for the dissipation of strain at the bonding area while reinforcing the first 90° layer, meaning that the printed line can withstand more strain before fracturing. In contrast, a 0−90 sample has 0° relative orientation angle, which does little to dissipate the stress on the 90° layer since it is directly perpendicular to the direction of strain. Therefore, the bonding between layers is easier to break compared to the 90−45 print pattern. In the 90−90 case, since the layers are parallel to each other, there is no longer a transverse layer that acts to dissipate the stress.

To demonstrate the effects of infill density on mechanical properties of printed porous PDMS, Young's modulus, UTS, and elongation at break of each print pattern at infill densities of 50, 75, and 100% were determined by tensile tests as shown in Figure 5 (each point was tested by three replicas and the averages were plotted). Figure 5a shows that Young's modulus increased 103% from an average of 2.18 MPa across six print patterns to 4.42 MPa as infill density increased from 50 to 75%. However, further increase of infill density to 100% decreased Young's modulus 45% to 3.05 MPa (see Supporting Information: Table S1). The increase in Young's modulus from 50 to 75% infill density can be attributed to an increase in the number of points of contact which allows for increased bonding between layers.[38] However, porous PDMS exhibits decreasing in Young's modulus from 75 to 100% infill density. It implies that the increased 25% infill density of material contributes not so much to decrease the voids between printed lines (as can be seen in Figure 4g).[43] We suspect that the presence of micron-sized pores in the PDMS matrix could become dominant in determining Young's modulus at 100% infill density, as it is known that Young's modulus would be exponentially decreased while the porosity increases.[44] To further verify our hypothesis, we prepared nonporous PDMS with silica NPs, silicone oil, and DBP as a control to study the micropores' effect on the obvious trend found at 75 and 100% infill density. The 90−90 print pattern was adopted as the design for the control sample because it showcases the highest value at 75% compared to 100% infill density across Young's modulus, UTS, and elongation at break. Interestingly, Young's modulus of nonporous PDMS with silica NPs, silicone oil, and DBP with the 90−90 print pattern at 75 and 100% infill density shows an opposite trend to porous PDMS, as it is slightly higher at 100% than 75% infill density with values of 0.88 and 0.83 MPa, respectively (Table S2). The result of this experiment indicates that highest Young's modulus of porous PDMS at 75% infill density can be attributable to the presence of micron-sized pores inside. Notably, the porous PDMS sample printed with 75% infill density shows the highest Young's modulus throughout all different print patterns. In fact, this result could propose a new perspective to save manufacturing time and materials since printed samples with 75% infill density have exhibited higher Young's modulus than 100% infill density samples.

Similarly, as seen in Figure 5b, the highest UTS (0.637 MPa) is shown in samples printed at 75% infill density, whereas 50 and 100% infill density samples exhibit 0.423 and 0.576 MPa, respectively (see Supporting Information: Table S3). The same trend was found in nonporous PDMS with silica NPs, silicone oil, and DBP with the 90−90 print pattern. The UTS at 75 and 100% infill density is 0.34 and 0.28 MPa, respectively, which indicates that the intrinsic material is dominant in determining the UTS at 100% infill density.[44] Figure 5d illustrates representative stress−strain curves of porous PDMS and nonporous PDMS with silica NPs, silicone oil, and DBP with a 90−90 print pattern for different infill densities, which clearly shows the trend that porous PDMS samples at 75% infill density yield the highest UTS and Young's modulus. On average, strain at break (Figure 5c) tends to increase when infill density increased from 50 to 75%, while slightly decreased from 75 to 100% infill density (see Supporting Information: Table S4). However, note that we could not observe obvious trends between elongation at break and infill density within each print pattern. According to this set of results, we could conclude that the mechanical properties of printed porous PDMS can be tuned solely based on infill density without changing the printing geometry or material composition. Namely, the material exhibits the highest stiffness and strength at 75% infill density, whereas infill density does not have a strong correlation with the capability of a porous material to sustain permanent deformation before fracture, as represented by the elongation at break values. We note that the tunable mechanical properties can be achieved by varying the infill densities and print patterns, and it offers great potential to applications that require the integration of different mechanical

https://doi.org/10.1021/acsapm.1c00417
ACS Appl. Polym. Mater. 2021, 3, 3496−3503

properties. Specifically, strength and stiffness can be locally controlled by varying either infill density or the print pattern (i.e., printing line angle or orientation), which not only greatly enlarges the design space but also offers a means to fabricate soft actuators and robots that encode different mechanical properties within a device composed of a single material.

CONCLUSIONS

We have studied the relationship between different print patterns and infill densities and their resulting mechanical properties of printed porous PDMS. The addition of DBP, silicone oil, and fumed silica NPs to the liquid PDMS precursor in a simple mixing process effectively tunes the rheological behavior to create a printable ink. Rheological characterization has shown that the porous PDMS ink exhibits shear thinning properties and a sufficient yield stress value of 200 Pa, which allows the material to be extruded via DIW and support the stacking of layers to maintain 3D structures. After printing and curing, the removal of DBP via immersion in ethanol generates micron-sized pores (1−10 μm in diameter) as examined by SEM imaging. We have shown that the resulting porous PDMS possesses significantly improved mechanical properties compared to nonporous PDMS, with a 378% increase in stiffness, 267% in strength, and 14% in ductility. The sole effect of micron-sized pores inside porous PDMS is further investigated and is found to contribute significantly to the enhanced mechanical properties compared to the addition of silica NPs. After comparing nonporous PDMS, porous PDMS and nonporous PDMS with silica NPs, silicone oil, and DBP samples, we have demonstrated the effects of infill density and print pattern on the mechanical properties of 3D-printed porous PDMS. Notably, tensile test results of different print patterns across 50, 75, and 100% infill densities showed that 75% infill density samples of porous PDMS yield the highest stiffness and strength. Among the different print patterns, the 90−45 samples exhibited the highest Young's modulus across 50, 75, and 100% infill densities. The porous PDMS elastomer offers tunable mechanical properties by varying infill densities and print patterns without changing the material system. We suspect that the findings in the work are highly applicable to the fields of soft robotics and biomedical devices that require fabricating complex structures and spatially integrating different mechanical properties into a single device using 3D printing techniques.

ASSOCIATED CONTENT

Supporting Information

The Supporting Information is available free of charge at https://pubs.acs.org/doi/10.1021/acsapm.1c00417.

Additional information on mechanical properties of the various printing patterns and infill densities (PDF)

PDMS and porous PDMS samples while printing (MP4)

Porous PDMS lattice structure while printing (MP4)

AUTHOR INFORMATION

Corresponding Author

Jinhye Bae − *Department of NanoEngineering, Chemical Engineering Program, Material Science and Engineering Program, and Sustainable Power and Energy Center (SPEC), University of California San Diego, La Jolla, California 92093, United States;* orcid.org/0000-0002-2536-069X; Email: j3bae@ucsd.edu

Authors

Rebekah Woo − *Department of NanoEngineering, University of California San Diego, La Jolla, California 92093, United States*

Grace Chen − *Department of NanoEngineering, University of California San Diego, La Jolla, California 92093, United States*

Jiayu Zhao − *Department of NanoEngineering, University of California San Diego, La Jolla, California 92093, United States*

Complete contact information is available at: https://pubs.acs.org/10.1021/acsapm.1c00417

Author Contributions

‡R.W., G.C., and J.Z. contributed equally to this work.

Notes

The authors declare no competing financial interest.

ACKNOWLEDGMENTS

R.W., G.C., and J.Z. contributed equally to this work. This work was supported by the National Science Foundation through the University of California San Diego Materials Research Science and Engineering Center (UCSDMRSEC), grant number DMR-2011924, with additional support from the University of California San Diego start-up fund. The authors thank Prof. Marc A. Meyers for allowing them to use the Instron testing machine and Prof. Karen Christman for allowing them to use the rheometer in their labs.

REFERENCES

(1) Rus, D.; Tolley, M. T. Design, Fabrication and Control of Soft Robots. *Nature* **2015**, *521*, 467−475.

(2) Eduok, U.; Faye, O.; Szpunar, J. Recent Developments and Applications of Protective Silicone Coatings: A Review of PDMS Functional Materials. *Prog. Org. Coat.* **2017**, *111*, 124−163.

(3) Liu, J.; Yao, Y.; Li, X.; Zhang, Z. Fabrication of Advanced Polydimethylsiloxane-Based Functional Materials: Bulk Modifications and Surface Functionalizations. *Chem. Eng. J.* **2021**, *408*, No. 127262.

(4) Chen, J.; Zheng, J.; Gao, Q.; Zhang, J.; Zhang, J.; Omisore, O.; Wang, L.; Li, H. Polydimethylsiloxane (PDMS)-Based Flexible Resistive Strain Sensors for Wearable Applications. *Appl. Sci.* **2018**, *8*, 345.

(5) Jeerapan, I.; Poorahong, S. Review—Flexible and Stretchable Electrochemical Sensing Systems: Materials, Energy Sources, and Integrations. *J. Electrochem. Soc.* **2020**, *167*, No. 037573.

(6) Tsao, C.-W. Polymer Microfluidics: Simple, Low-Cost Fabrication Process Bridging Academic Lab Research to Commercialized Production. *Micromachines* **2016**, *7*, 225.

(7) Tang, S. K. Y.; Whitesides, G.M. *Basic Microfluidic and Soft Lithographic Techniques.*

(8) Bergeron, V.; Cooper, P.; Fischer, C.; Giermanska-Kahn, J.; Langevin, D.; Pouchelon, A. Polydimethylsiloxane (PDMS)-Based Antifoams. *Colloids Surf. A Physicochem. Eng. Asp.* **1997**, *122*, 103−120.

(9) Hong, Y.; Zhou, J. G.; Yao, D. Fabrication of Interconnected Porous Elastomers by a Microsphere-Templating Process. *Adv. Polym. Technol.* **2013**, *32*, No. 21330.

(10) Xu, Y.; Sun, B.; Ling, Y.; Fei, Q.; Chen, Z.; Li, X.; Guo, P.; Jeon, N.; Goswami, S.; Liao, Y.; Ding, S.; Yu, Q.; Lin, J.; Huang, G.; Yan, Z. Multiscale Porous Elastomer Substrates for Multifunctional On-Skin Electronics with Passive-Cooling Capabilities. *Proc. Natl. Acad. Sci. U. S. A.* **2020**, *117*, 205−213.

(11) Moraleda, J.; Segurado, J.; Llorca, J. *Finite Deformation of Porous Elastomers: A Computational Micromechanics Approach*; Madrid, 2007.
(12) Yu, C.; Yu, C.; Cui, L.; Song, Z.; Zhao, X.; Ma, Y.; Jiang, L. Facile Preparation of the Porous PDMS Oil-Absorbent for Oil/Water Separation. *Adv. Mater. Interfaces* **2017**, *4*, No. 1600862.
(13) Gale, B.; Jafek, A.; Lambert, C.; Goenner, B.; Moghimifam, H.; Nze, U.; Kamarapu, S. A Review of Current Methods in Microfluidic Device Fabrication and Future Commercialization Prospects. *Inventions* **2018**, *3*, 60.
(14) Faustino, V.; Catarino, S. O.; Lima, R.; Minas, G. Biomedical Microfluidic Devices by Using Low-Cost Fabrication Techniques: A Review. *J. Biomech.* **2016**, *49*, 2280−2292.
(15) Yazdi, A. A.; Popma, A.; Wong, W.; Nguyen, T.; Pan, Y.; Xu, J. 3D Printing: An Emerging Tool for Novel Microfluidics and Lab-on-a-Chip Applications. *Microfluid. Nanofluid.* **2016**, *20*, 50.
(16) Bhattacharjee, N.; Urrios, A.; Kang, S.; Folch, A. The Upcoming 3D-Printing Revolution in Microfluidics. *Lab Chip* **2016**, *16*, 1720−1742.
(17) Lewis, J. A. Direct Ink Writing of 3D Functional Materials. *Adv. Funct. Mater.* **2006**, *16*, 2193−2204.
(18) Barnes, H. A. Thixotropy - A Review. *J. Non-Newtonian Fluid Mech.* **1997**, *70*, 1−33.
(19) Wehner, M.; Truby, R. L.; Fitzgerald, D. J.; Mosadegh, B.; Whitesides, G. M.; Lewis, J. A.; Wood, R. J. An Integrated Design and Fabrication Strategy for Entirely Soft, Autonomous Robots. *Nature* **2016**, *536*, 451−455.
(20) Qin, Z.; Compton, B. G.; Lewis, J. A.; Buehler, M. J. Structural Optimization of 3D-Printed Synthetic Spider Webs for High Strength. *Nat. Commun.* **2015**, *6*, 1−7.
(21) Kolesky, D. B.; Homan, K. A.; Skylar-Scott, M. A.; Lewis, J. A. Three-Dimensional Bioprinting of Thick Vascularized Tissues. *Proc. Natl. Acad. Sci. U. S. A.* **2016**, *113*, 3179−3184.
(22) Paquien, J. N.; Galy, J.; Gérard, J. F.; Pouchelon, A. Rheological Studies of Fumed Silica-Polydimethylsiloxane Suspensions. *Colloids Surf. A Physicochem. Eng. Asp.* **2005**, *260*, 165−172.
(23) Wu, A. S.; Small, W.; Bryson, T. M.; Cheng, E.; Metz, T. R.; Schulze, S. E.; Duoss, E. B.; Wilson, T. S. 3D Printed Silicones with Shape Memory. *Sci. Rep.* **2017**, *7*, 1−6.
(24) Chen, Q.; Zhao, J.; Ren, J.; Rong, L.; Cao, P.; Advincula, R. C. 3D Printed Multifunctional, Hyperelastic Silicone Rubber Foam. *Adv. Funct. Mater.* **2019**, *29*, No. 1900469.
(25) Roh, S.; Parekh, D. P.; Bharti, B.; Stoyanov, S. D.; Velev, O. D. 3D Printing by Multiphase Silicone/Water Capillary Inks. *Adv. Mater.* **2017**, *29*, No. 1701554.
(26) Mea, H. J.; Delgadillo, L.; Wan, J. On-Demand Modulation of 3D-Printed Elastomers Using Programmable Droplet Inclusions. *Proc. Natl. Acad. Sci. U. S. A.* **2020**, *117*, 14790−14797.
(27) Schumacher, C.; Bickel, B.; Rys, J.; Marschner, S.; Daraio, C.; Gross, M. Microstructures to Control Elasticity in 3D Printing. *ACM Trans. Graphics* **2015**, *34*, 1−13.
(28) Hinton, T. J.; Hudson, A.; Pusch, K.; Lee, A.; Feinberg, A. W. 3D Printing PDMS Elastomer in a Hydrophilic Support Bath via Freeform Reversible Embedding. *ACS Biomater. Sci. Eng.* **2016**, *2*, 1781−1786.
(29) Ozbolat, V.; Dey, M.; Ayan, B.; Povilianskas, A.; Demirel, M. C.; Ozbolat, I. T. 3D Printing of PDMS Improves Its Mechanical and Cell Adhesion Properties. *ACS Biomater. Sci. Eng.* **2018**, *4*, 682−693.
(30) Lewis, J. A.; Gratson, G. M. Direct Writing in Three Dimensions. *Mater. Today* **2004**, *7*, 32−39.
(31) M'Barki, A.; Bocquet, L.; Stevenson, A. Linking Rheology and Printability for Dense and Strong Ceramics by Direct Ink Writing. *Sci. Rep.* **2017**, *7*, 1−10.
(32) Azad, M. A.; Olawuni, D.; Kimbell, G.; Badruddoza, A. Z. M.; Hossain, M. S.; Sultana, T. Polymers for Extrusion-Based 3D Printing of Pharmaceuticals: A Holistic Materials−Process Perspective. *Pharmaceutics* **2020**, *12*, 124.
(33) Johnston, I. D.; McCluskey, D. K.; Tan, C. K. L.; Tracey, M. C. Mechanical Characterization of Bulk Sylgard 184 for Microfluidics and Microengineering. *J. Micromech. Microeng.* **2014**, *24*, No. 035017.
(34) Wang, X.; Zhao, L.; Fuh, J. Y. H.; Lee, H. P. Effect of Porosity on Mechanical Properties of 3D Printed Polymers: Experiments and Micromechanical Modeling Based on X-Ray Computed Tomography Analysis. *Polymer* **2019**, *11* () DOI: 10.3390/polym11071154.
(35) Rezanezhad, M.; Lajevardi, S. A.; Karimpouli, S. Effects of Pore (s)-Crack Locations and Arrangements on Crack Growth Modeling in Porous Media. *Theor. Appl. Fract. Mech.* **2020**, *107*, No. 102529.
(36) N. J., Holzman. *3D Printing and Mechanical Performance of Silicone Elastomers*, The University Of Minnesota, 2019.
(37) Aloyaydi, B.; Sivasankaran, S.; Mustafa, A. Investigation of Infill-Patterns on Mechanical Response of 3D Printed Poly-Lactic-Acid. *Polym. Test.* **2020**, *87*, No. 106557.
(38) Yun Aw, Y.; Keat Yeoh, C. I.; Asri Idris, M.; Leng Teh, P.; Amali Hamzah, K.; Aqzna Sazali, S. Effect of Printing Parameters on Tensile, Dynamic Mechanical, and Thermoelectric Properties of FDM 3D Printed CABS/ZnO Composites. *Materials* **2018**, *11*, 14.
(39) Kiendl, J.; Gao, C. Controlling Toughness and Strength of FDM 3D-Printed PLA Components through the Raster Layup. *Compos. Part B Eng.* **2020**, *180*, No. 107562.
(40) Jiang, S.; Liao, G.; Xu, D.; Liu, F.; Li, W.; Cheng, Y.; Li, Z.; Xu, G. Mechanical Properties Analysis of Polyetherimide Parts Fabricated by Fused Deposition Modeling. *High Perform. Polym.* **2019**, *31*, 97−106.
(41) Dudescu, C.; Racz, L. Effects of Raster Orientation, Infill Rate and Infill Pattern on the Mechanical Properties of 3D Printed Materials. *ACTA Univ. Cibiniensis* **2017**, *69*, 23−30.
(42) You, F.; Wu, X.; Chen, X. 3D Printing of Porous Alginate/Gelatin Hydrogel Scaffolds and Their Mechanical Property Characterization. *Int. J. Polym. Mater. Polym. Biomater.* **2017**, *66*, 299−306.
(43) Terekhina, S.; Skornyakov, I.; Tarasova, T.; Egorov, S. Effects of the Infill Density on the Mechanical Properties of Nylon Specimens Made by Filament Fused Fabrication. *Technologies* **2019**, *7*, 57.
(44) Wang, J. C. Young's Modulus of Porous Materials - Part 1 Theoretical Derivation of Modulus-Porosity Correlation. *J. Mater. Sci.* **1984**, *19*, 801−808.

https://doi.org/10.1021/acsapm.1c00417
ACS Appl. Polym. Mater. 2021, 3, 3496−3503